The Canadian society for engineering in agricultural, food, and biological systems

CSAE SCGR

La société canadienne de génie agroalimentaire et biologique

Paper No. 05-041

INTELLIGENT COMPUTER VISION SYSTEM (SAIF) FOR AUTOMATED INSPECTION OF GINSENG ROOTS QUALITY

A. I. Martynenko

School of Engineering, University of Guelph

Guelph ON, N1G 2W1 e-mail: omartyne@uoguelph.ca

V.J. Davidson

School of Engineering, University of Guelph

Guelph ON, N1G 2W1 e-mail: vdavidso@uoguelph.ca

R. B. Brown

School of Engineering, University of Guelph

Guelph ON, N1G 2W1 e-mail: rbbrown@uoguelph.ca

Written for presentation at the
CSAE/SCGR 2005 Meeting
Winnipeg, Manitoba
June 26 - 29, 2005

Abstract

Intelligent computer-vision system for automated inspection of food safety and quality (SAIF) developed on the basis of compact CCD camera with IEEE-1396 interface and configurable software (IMAQ^{TM}6.1, Lab VIEW 7.0) is presented. It offers an extensive set of optimized functions for advanced image acquisition, segmentation, feature extraction, data analysis, spatial measurement and calibration. It also includes the ability to set up complex pass/fail decisions in order to control digital I/O devices such as PLC. The system application for online inspection of ginseng root quality during drying was developed. Area shrinkage was continuously monitored through computer-vision system by extracting morphological features with thresholding and pixels counting. Colour changes were monitored through computer-vision system as surface color intensity. Relationships between image attributes and physical parameters of drying (shrinkage/moisture, color/quality) were used for online estimation of actual moisture content and quality degradation. Testing of system proved accuracy in estimation of ginseng quality and process parameters in multi-stage drying. The feasibility of SAIF as system observer for closed-loop control is discussed.

Keywords: ginseng, shrinkage, colour, texture, quality, machine-vision, inspection, control.

1. Introduction

The use of computer vision for automated food inspection keeps on growing *(Batchelor et al.,1985, Zuech, 1990, Gunasekaran, 2000, Lu, Wen, 2000, Sun, 2000).* Quantification of morphological, colour and textural features enabled to develop advanced algorithms for classification of grain (*Majumdar & Jayas, 2000a-d; Paliwal et al., 2001*), fruits (*Leemans et al, 2002; Blasco et al., 2003*) and vegetables (*Tao et al., 1990; Nilsen et al., 1998*). Recent advances in multi-layer neural networks essentially improved performance of computer-vision classifiers (*Jayas et al., 2000; Paliwal et al.*, *2003*). However, because of features correlation, it can decline the performance of the classifier (*Mujumdar & Jayas, 2000d*). Selection the minimal set of non-correlated features, sufficient for discrimination of object/process attributes in informational space, is one of the most important elements of image analysis (*Klir, 1985*). It requires careful image pre-processing: segmentation, pixel clustering, and optimal thresholding (*DaFontoura & Marcondes, 2001*), combined with advanced data analysis *(Blasco et al, 2003)* or pattern classification *(Jayas et al., 2000).*

Computer vision offers a tremendous resolution for monitoring of spatial and temporal changes in food processing *(Fernandez et al., 2005)*. However, the gap between image attributes and physical parameters (moisture, quality, temperature) essentially limits applications of computer vision for industrial purposes.

The objective of this study was automated inspection of ginseng root quality, which is the critical issue in ginseng root drying *(Davidson et al., 2004).* Ginseng quality was specified as desirable color, texture and moisture content *(Grade and Quality Standards of Products of Processed American ginseng, 1998).* To achieve the objective, the procedures of image segmentation, feature extraction and data analysis were developed. Relationships between image attributes and physical parameters of drying (moisture and quality) were established.

2. Materials and methods

2.1. Drying chamber

Experiments were carried out in a specially designed drying chamber (Figure 1). For automated inspection of visual color and area changes during drying the chamber was made up of a 300 mm length of Plexiglas tube with an inside diameter of 120 mm. It was connected to an air conditioning unit that produced constant airflow with regulated temperature and humidity. Temperatures of air and root surface were measured with identical T-type thermocouples with a spherical junction 0.85mm in diameter.

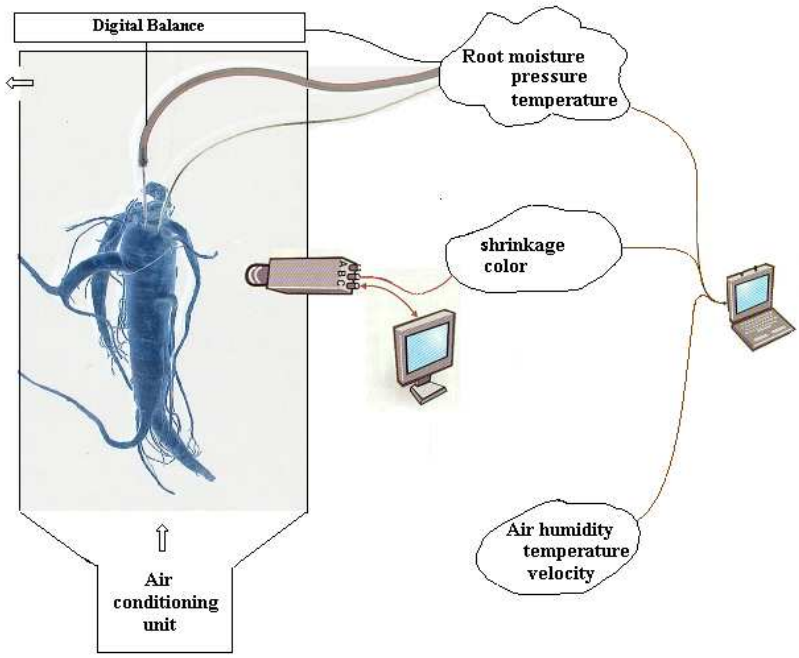

Figure 1. Experimental drying chamber with computer-vision system

For measurement of temperatures inside of the root hypodermic Teflon-insulated microprobes 0.65mm in diameter were used. Measurements with the thermocouples were made using an interface card[1] with built in cold-junction compensation in the control computer. Based on the calibration, absolute error associated with the thermocouple measurements was $\pm 0.1^{o}C$ and the relative error between measurements was $\pm 0.05^{o}C$.

[1] Model PCI-20303T, Intelligent Instrumentation Inc., Tucson, Arizona 85706, USA

Air relative humidity was measured using a humidity sensor[2] with a sensitivity of 25mV/% RH and an accuracy of 2%. Airflow rate was measured with an anemometer[3] with an accuracy of 5%. Root weight was measured continuously with a digital balance with a serial interface to the control computer. Data from the thermocouples, humidity sensors and the digital balance were recorded continuously by National Instruments' Lab VIEW 7.0™ through a data acquisition interface card[4].

2.2. Samples

The ginseng root samples used in this study was obtained from Hare Farms (Waterford, Ontario) in October 2003 and October 2004. Both harvests were taken from four-year ginseng plots. Ginseng population contained roots of different shapes and sizes in the range from 4 to 40mm in diameter. Fresh ginseng roots were stored in a refrigerator at 5±2°C during the experimental study period (3 months). Prior to each drying experiment, roots were washed and care was taken to drain the roots and remove wash water.

2.3. Computer vision system

The hardware consisted of a portable compact CCD camera[5] with built-in 4.65 mm lens with anti-reflective coating connected to a personal computer (P4, 2.4GGz) using PCI IEEE-1394 FireWire adapter[6]. The software consisted of NI-IMAQ data acquisition driver for IEEE-1394, LabVIEW 7.0 and IMAQ6.1™ Vision Builder[7]. Camera and data acquisition interface were configured with NI-MAX (Measurement and Automation Explorer). Digital camera was mounted in on a vertical stand, which provided easy vertical movement and stable support for the camera. The depth of field was enough to obtain quality images with a high contrast of boundaries and high color resolution. The image

[2] Model HIH-3602C, Honeywell Inc., 101 Columbia Road Morristown, NJ 07962 USA
[3] Davis Instruments Corp., 3465 Diablo Ave., Hayward, CA 94545, USA
[4] Model NI PCI-6220, National Instruments, Austin, Texas, USA
[5] Model Fire-i, Unibrain Inc., P.O. Box 203730 Austin, Texas 78720-3730, USA
[6] Model FWPCI-3 PCI IEEE-1394 OHCI adapter, Unibrain Inc., USA
[7] National Instruments, Austin, Texas, USA

resolution was 0.1 mm/pixel and 0.08 mm/pixel in the horizontal and vertical directions, respectively. 24-bit RGB-images were converted to square pixels with the resolution 0.01mm^2/pixel. Uniform illumination was provided with SYLVANIA CF15EL/830 diffuse fluorescent bulbs with corrected color temperature of 4200^{o}K and a color reproduction index near to 95%. Image capturing, processing and subsequent analysis were performed online using LabVIEW graphical interface.

2.4. Image analysis

Image analysis included image segmentation, features extraction and data analysis. Image segmentation was designed to separate region of interest (ROI) from background. Extraction of morphological, colour and textural features was provided every hour with the library of virtual instruments, embedded in NI-IMAQ6.1 Visual Builder. Image features, determined as time-dependent variables, were used further in data analysis to calculate physical (moisture and quality) and rate (drying rate, quality degradation) parameters of drying.

2.4.1. Image Segmentation

The first step of image analysis was image segmentation. This algorithm, based on edge detection, operated by finding the optimal threshold that minimizes the entropy of the fuzziness measure[8]. For ginseng root it was found that the red channel of RGB colour space provided the best discrimination between reflectance properties of ginseng surface and background. The output [0,256] gray image was converted then into binary [0,1] image with 1s assigned to ginseng root and 0s assigned to background. This binary image was used for two purposes: a) estimation of morphological features and b) masking original color image for extraction of color and textural features. Multiplication of original image

[8] This procedure was found more consistent than automatic thresholding technique (*Parker, 1994*) or truncation of "dark" intensity pixels below 50 (*Fernandez et al., 2005*)

on its binary mask enabled to convert all background pixels to zero intensity pixels and eliminate this class from next calculations.

The block-scheme of image segmentation procedure is shown in Figure 2.

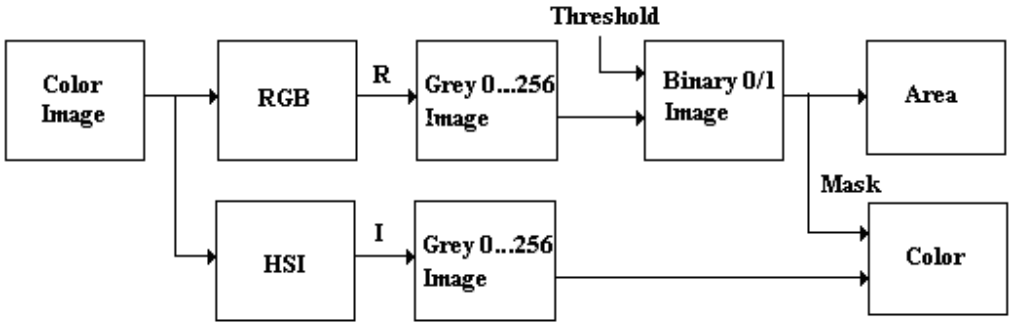

Figure 2. Image segmentation procedure

Original color image was filtered twice: in RGB colour space to extract morphological features and in HSI (hue-saturation-intensity) colour space to extract colour features.

2.4.2. Feature Extraction

Morphological features:

The software library enabled to extract all morphological features: surface area, length, width, radius, shape factor and their statistical (mean and variance) characteristics. However, not all of them were used in the next data analysis. Length-to-width ratio was used for identification of root orientation in XOZ plane. Surface area was used for identification of moisture content *(Davidson et al., 2004).* To distinguish root area from isolated small clusters of pixels, the procedure of multi-threshold filtering with next particle analysis was applied. Root area was determined as the largest object on the binary image. Overall surface area was obtained by conversion of "1"pixels of binary image into area through conversion coefficient 0.01mm^2/pixel with the next multiplication on π (cylindrical root geometry).

Colour features:

Color features were extracted as means and variances of red (R), green (G) and blue (B) channels in RGB colour space and color intensity (I) in HSI colour space. To avoid effects of size sampling on colour intensity distribution, the number of pixels for each intensity line was normalized with respect to overall number of pixels in extracted area. The histogram of color intensity was treated as a fuzzy variable with lightness as a support. Average color intensity was calculated from color intensity histogram on the basis of center-of-gravity defuzzification *(Jang et al., 1997)*. Means and variances were used to test statistical hypothesis (F-test) about color changes on each interval of observation.

Textural features:

Texture recognition was carried out by means of co-occurrence matrix (COM) *(Mujumdar & Jayas, 2000c).* The pattern of intensity pixels in XOZ image plane was characterized with non-uniform distribution in radial (X) and axial (Z) directions. Hence, ginseng root texture was calculated as a geometry-related feature in two directions: across root (radial profile) and along root (axial profile) by using methods of statistical identification, such as autocorrelation $R_{xx}(\tau)$, $R_{zz}(\tau)$, and spectral power density $S_{xx}(\omega)$, $S_{zz}(\omega)$ functions. Spectral power density was calculated by using FFT for one-dimensional colour intensity profile the same way as a two-dimensional co-occurrence matrix *(Paliwal et al., 2003, Fernandez et al., 2005)*. Spectral power density enables to get information not only about homogeneity of pixels distribution, but also about some periodical attributes of ginseng surface, such as surface wrinkling. First peak of spectral power density was used to measure textural uniformity. Second peak and higher harmonics of spectral power characterized development of regular wrinkles on the root surface.

Energy was calculated as an integral of spectral power density:

$$E = \int_0^{\omega} S(\omega) d\omega \qquad (1)$$

where ω (pixels^{-1}) was reciprocal to the distance between pixels. Calculated energy was a measure of textural uniformity and decreased dramatically during drying.

The flow chart of feature extraction is shown in Figure 3.

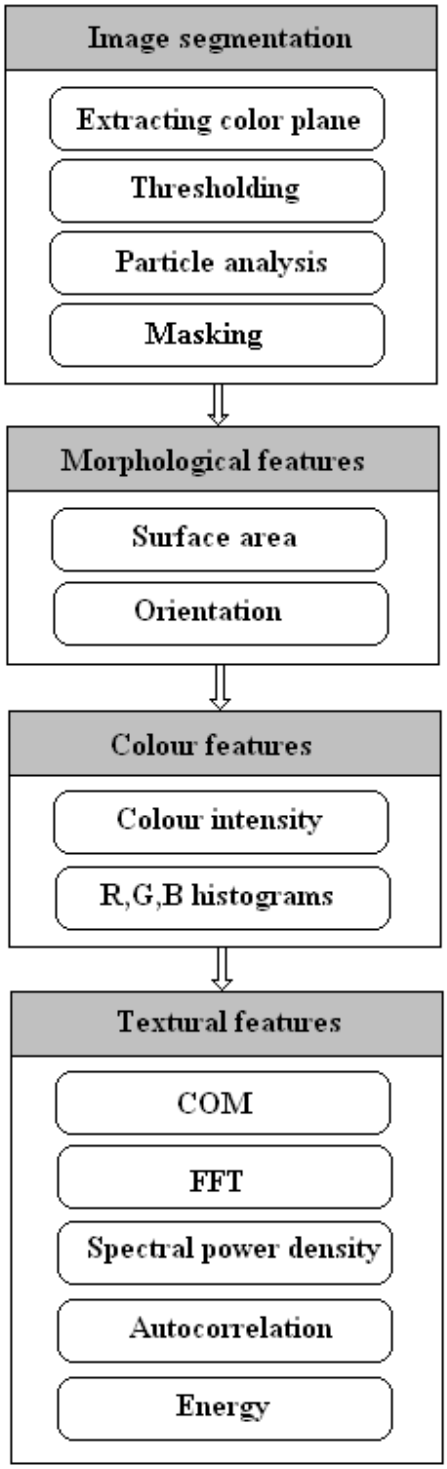

Figure 3. Flow chart of feature extraction

2.4.3. Data analysis

Data analysis was provided to relate the set of morphological, colour and textural features with the set of physical parameters of ginseng root quality. In informational space the object system appears as a set of attributes, each associated with a set of appearances, and a set of domains, each associated with a set of its elements (Klir, 1985). It can be expressed as:

$$O = (\{(a_i, A_i)\big|_{i=1,2,..n}\}, \{(b_j, B_j)\big|_{j=1,2,...m}\}) \quad (2)$$

where a_i, A_i denote an attribute and a set of its appearances, respectively,

b_j, B_j denote a domains and a set of its elements.

Three important attributes of ginseng root quality $\{a_1, a_2, a_3\}$ are moisture, quality and wrinkles *(Grade and Quality Standards of Products of Processed American ginseng, 1998)*. Two important domains $\{b_1, b_2\}$ are time and moisture content. Observation channel is the operation o_i, by which a specific variable is appeared as an image of an attribute a_i in a set of appearances A_i:

$$o_i : a_i \rightarrow A_i \quad (3)$$

Relationship between image attributes, measured on the time basis, and physical parameters are shown in Figure 4.

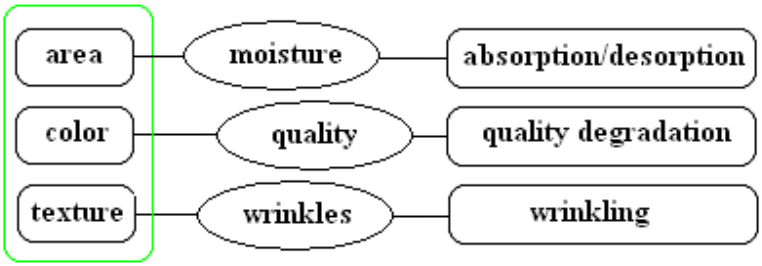

Figure 4. Relationships between image attributes, measured on the time basis, physical parameters and processes.

Three channels of observation were independent, delivering information about morphological, color and textural image attributes of object system. The accuracy of the computer vision system was evaluated as errors in area, colour and texture estimation. The error in area estimation due to isolated or small clusters of pixels, mainly located at the boundaries of adjacent regions was evaluated by comparison of binary images, obtained with original low-resolution (640x480) portable CCD camera and reference high-resolution (1392x1040) CCD camera[9] with a automatic adjustment of white balance and 25mm F/1.4 Mega Pixel Iris[10] lens.

The error in colour estimation was evaluated by comparing standard colour indices from bright yellowish to beige, corresponding to colour of ginseng roots. These indices were calculated in XYZ colour space, provided by standard colourimeter[11]. To avoid possible effects of non-uniform lighting, each sample was imaged three times for different angle orientation of roots (0, 120^o, 240^o) in the plane of measurement. The colour was calculated as the average of three measurements.

The error in texture estimation was evaluated by using of set of samples with calibrated grids of different sizes. Performance in estimation of periodical components was estimated as a signal-to-noise ratio in power spectrum density function, calculated with FFT.

All experiments were carried out with three replications in a random order to exclude the influence of uncontrolled changes during storage, including ageing and moisture loss. The correlations between morphological, color and textural features were tested with cross-correlation analysis (SAS6.0). Significance of features and their interactions was tested by standard ANOVA procedures. Adequacy of linear relationships between image attributes and physical parameters was tested on the basis of Fisher criteria with 0.95-confidence level.

[9] Model DFW-SX900, Sony Corporation, Japan
[10] Model 23FM25SP, Tamron USA Inc., 10 Austin Blvd., Commack, NY 11725, USA
[11] Minolta CR-300, Japan

3. Results and Discussion

3.1. Image segmentation

An example of image segmentation is presented in Figure 5. Original image of ginseng root with background noise, obtained with CCD color camera (Fig. 5a) was filtered in red with thresholding to obtain raw binary image (not shown). Subsequent cluster analysis was provided to select the region of interest (ROI) as the largest cluster in the image and eliminate small clusters, not belonging to ROI. Corrected binary image (Fig. 5b) was used as the mask to obtain original colour image with ideal (0s) background (Fig. 5c).

a)

b)

c)

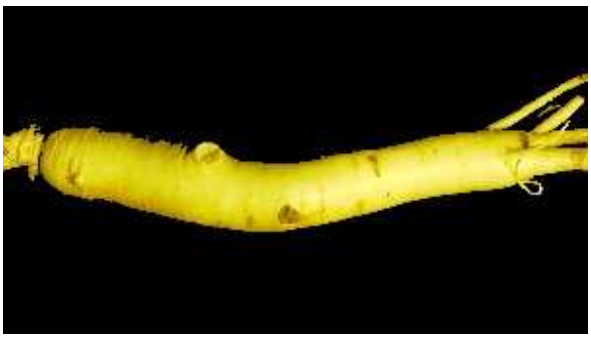

Figure 5. Image segmentation: a) original colour image of 20mm ginseng root, b) binary image after correction, c) original colour image after masking

3.2. Morphological features (shrinkage)

Surface area of the root was calculated from binary image (Fig. 5b) by conversion of pixels into area through multiplication on conversion coefficient 0.01 mm^2/pixel. Structural changes in ginseng root during drying were accompanied by volumetric shrinkage and a decrease in projected area. Area shrinkage $\xi(t)$ was calculated as dimensionless time-dependent variable, indicating shrinkage of surface area with time of drying. Taking into account surface area at equilibrium A_e the shrinkage is:

$$\xi_i = \frac{A_i - A_e}{A_o - A_e} \tag{4}$$

Area shrinkage of ginseng root (Figure 5) during 100 hours of drying at temperature 38°C, relative humidity 12% and airflow rate 1m/s is presented in Figure 6a.

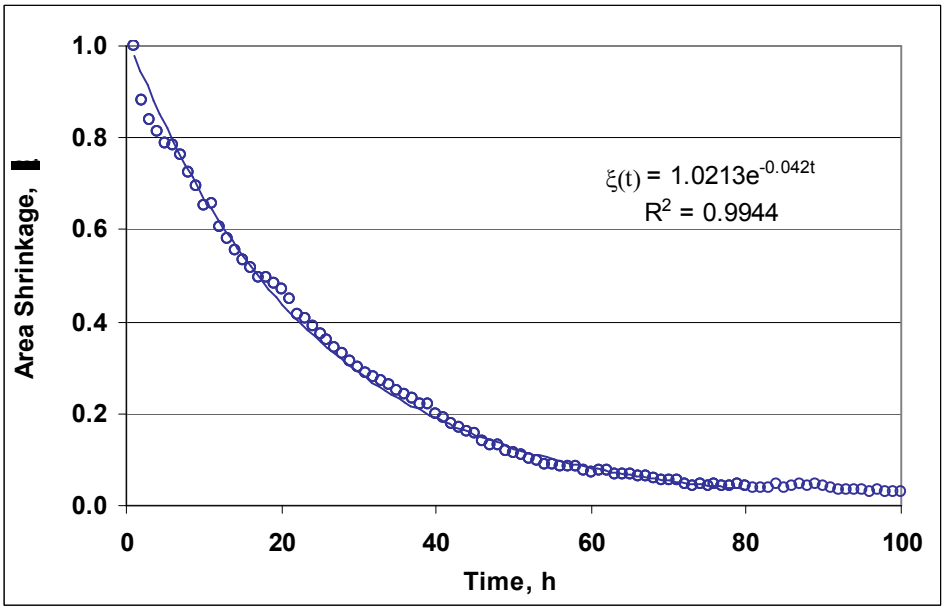

Figure 6a. Kinetics of area shrinkage in drying process (circles – points of observation, solid line – exponential fit)

Kinetics of shrinkage followed exponential behaviour in all experiments over the range of experimental conditions from 38°C to 50°C of temperatures, from 12 to 25% of

relative humidity and air velocity from 1m/s to 3m/s. In time domain it could be expressed as an exponential model:

$$\xi(t) = \exp^{-k_S t} \tag{4}$$

This exponential behaviour of area shrinkage during drying was in a good agreement with previous results (Li, 2002). Coefficient of determination (0.995) of exponential model reflected accuracy of image analysis for surface area estimation.

Area shrinkage, plotted in moisture domain, showed linear behaviour (Figure 6b). This linear relationship between dimensionless values of area shrinkage and moisture

$$\psi = a\xi \tag{5}$$

was valid for the most period of drying (R^2=*0.97*, standard error *0.016*).

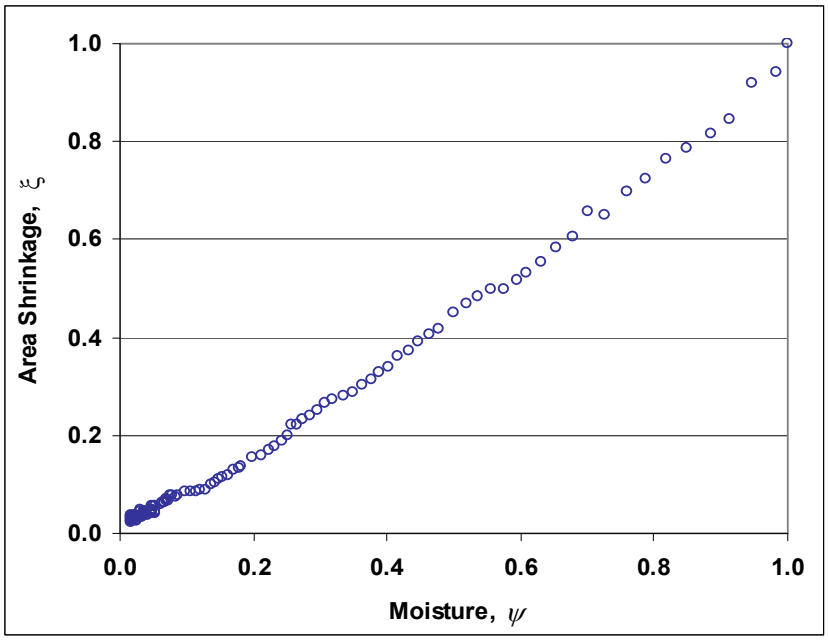

Figure 6b. Relationship between area shrinkage and moisture ratio

This correlation between shrinkage and moisture content in the range of moisture from initial to 0.3g/g (db) can be related to phenomenon of free water evaporation *(Ratti, 1994)*. However, below 0.3g/g area shrinkage cannot be used as the predictor of moisture losses.

3.3. Color features (color intensity)

Color intensity was extracted as a mean value of histogram of colour intensity distribution in HSI colour space (see section 2.4.2). Kinetics of colour changes in time and moisture domains are presented in Figure 7.

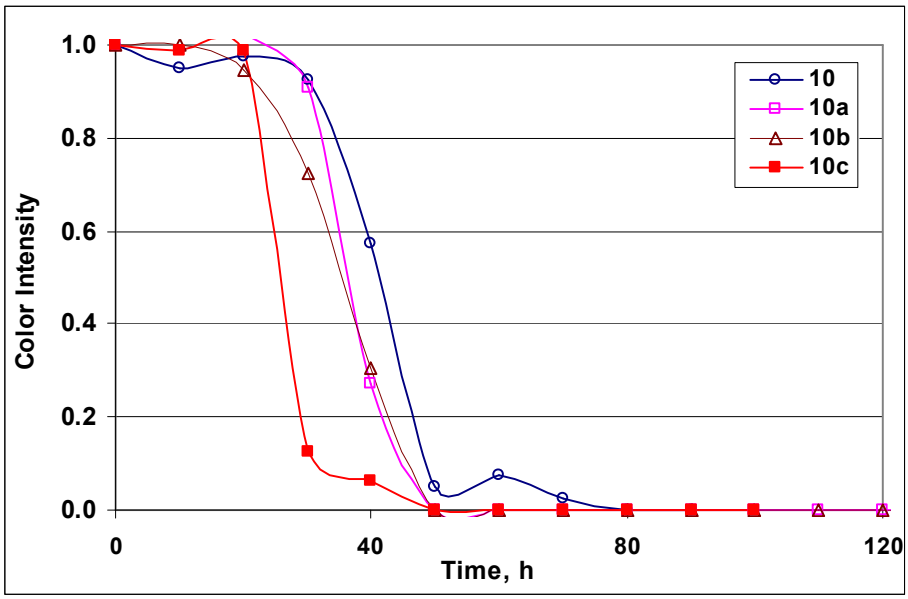

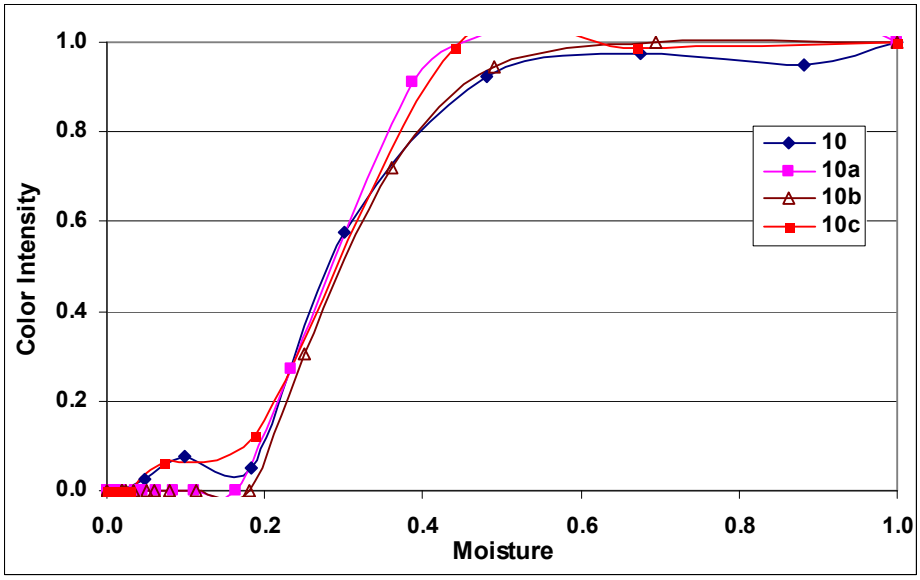

Figure 7. Color changes of ginseng root at 50°C temperature, 1m/s air velocity and 12% of relative humidity: a) in time domain; b) in moisture domain.

The most significant colour changes occurred between 30 and 50 hours of drying, starting at 0.5 and ending at 0.2 of moisture content. In moisture domain the variation between experiments was minimal. It follows that color intensity was moisture dependent, decreasing dramatically at the range of (0.5-0.2) of moisture content. This range of water activities corresponds to the maximal rate of Maillard reaction of non-enzymatic browning.

Color changes measured by image analysis and standard colorimeter (Minolta CR-300) gave high average correlation with $R^2=0.95$. These results were similar to those, reported for chromatic parameters "a" and "b" in Lab colour space, reported by Krokida *et al.* (2001) and Fernandez *et al.* (2005). It follows that color intensity can be used for monitoring of quality degradation in ginseng drying.

3.4. Textural features

Textural features of ginseng root surface were measured from colour intensity profile, which was computed separately for R, G and B color plane. Taking into account non-uniform texture of ginseng root in axial and radial directions, colour intensities were scanned in both longitudinal (z) and transverse (x) spatial coordinates on XOZ image plane.

Spatial distribution of colour intensities of fresh and dry roots in longitudinal direction (along root surface) is shown on Figure 8. There was significant anisotropy of textural features, which can be related to structural organization of ginseng root (for fresh root) and non-uniform longitudinal and radial shrinkage (for dry root).

Color profile of fresh root (Figure 8a) was characterized with saturation of red (255), high level of green (250±5), and average level of blue (140±10). Figure 8a shows uniform texture of fresh root surface with constant color distribution along the root. Textural non-regularities on longitudinal profile were not identifiable.

Color profile of dry root (Figure 8b) reflected more textural non-regularities of root after drying with local irregularities about 30-40pixels of size. They become observable at 0.5

of moisture content and were associated with wrinkles, which appeared on the root surface as the result of critical root shrinkage. These textural features were best identifiable from colour intensity profile in blue plane.

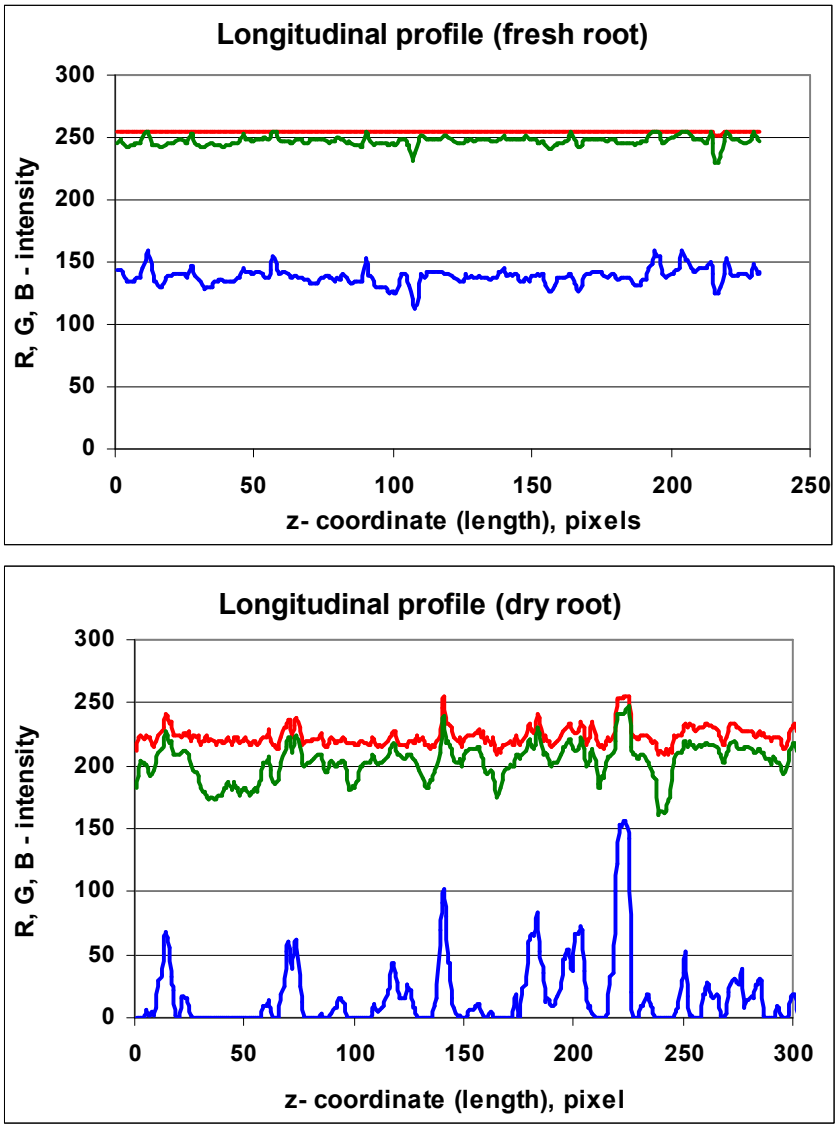

Figure 8. Textural profile of fresh (a) and dry (b) ginseng root (longitudinal scan)

From Figure 8 follows that drying causes substantial decreasing of mean values of colour intensities: red from 255 to 225; green from 250 to 200 and blue from 145 to 25. The most significant changes occur in blue color plane. A local irregularity with a random distribution appears at some point of drying as the result of surface shrinkage. The variability of color intensity profile was increased from red to blue.

Spatial distribution of colour intensities of fresh and dry roots in transverse direction (across root surface) is shown in Figure 9.

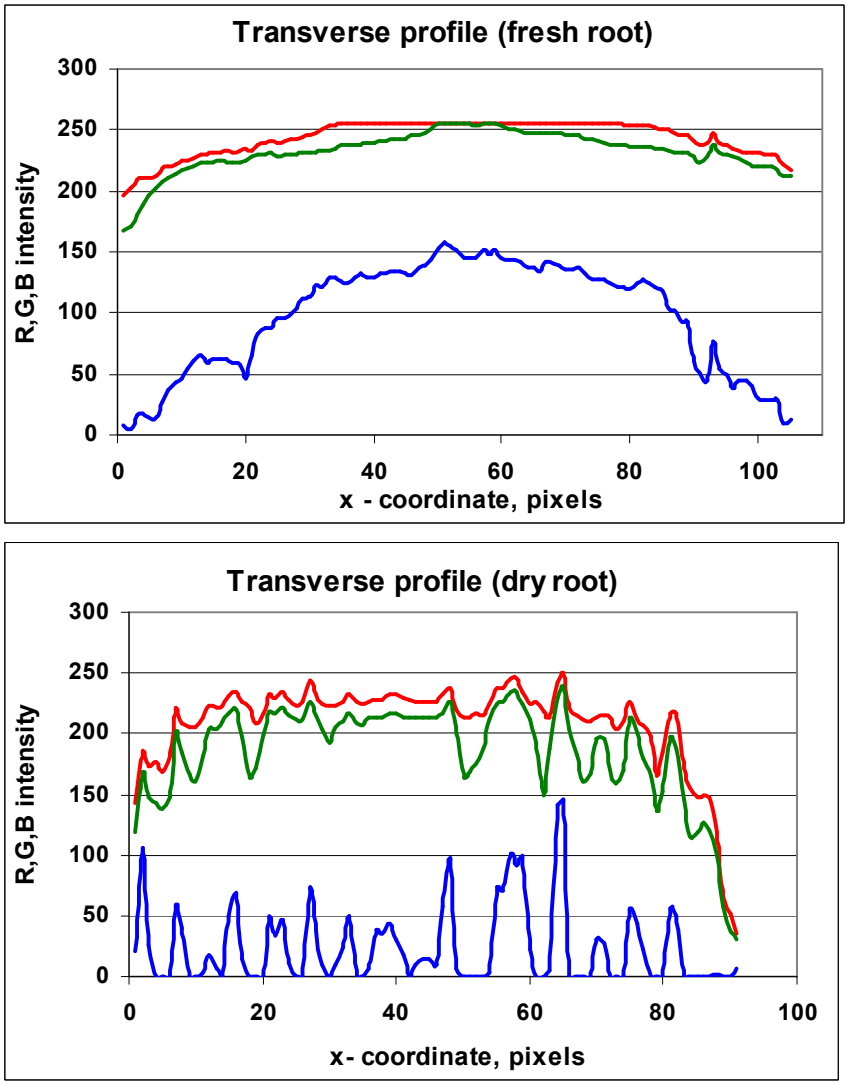

Figure 9. Textural profile of fresh (a) and dry (b) ginseng root (transverse scan)

Figure 9a shows uniform texture of fresh root. R, G and B color intensities were maximal in the center, decreasing on the root boundaries. This effect was related to root size and caused by non-uniform illumination of cylindrical root body with remote source of illumination. The magnitude of color changes was maximal in blue, being sensitive to local textural irregularities.

The higher harmonics, appearing on the root image after 20h of drying (Figure 9b), are the result of surface structural changes (wrinkling). These wrinkles with characteristical size 10 pixels (~1mm) are important attribute of root quality.

Textural features were quantified as spectral power density (measure of textural uniformity). Each textural feature was computed separately for R, G and B intensity plane as a function of a distance between pixels. Calculated values of spectral power density were normalized and presented on Figure 10 in spatial (frequency) and time domains.

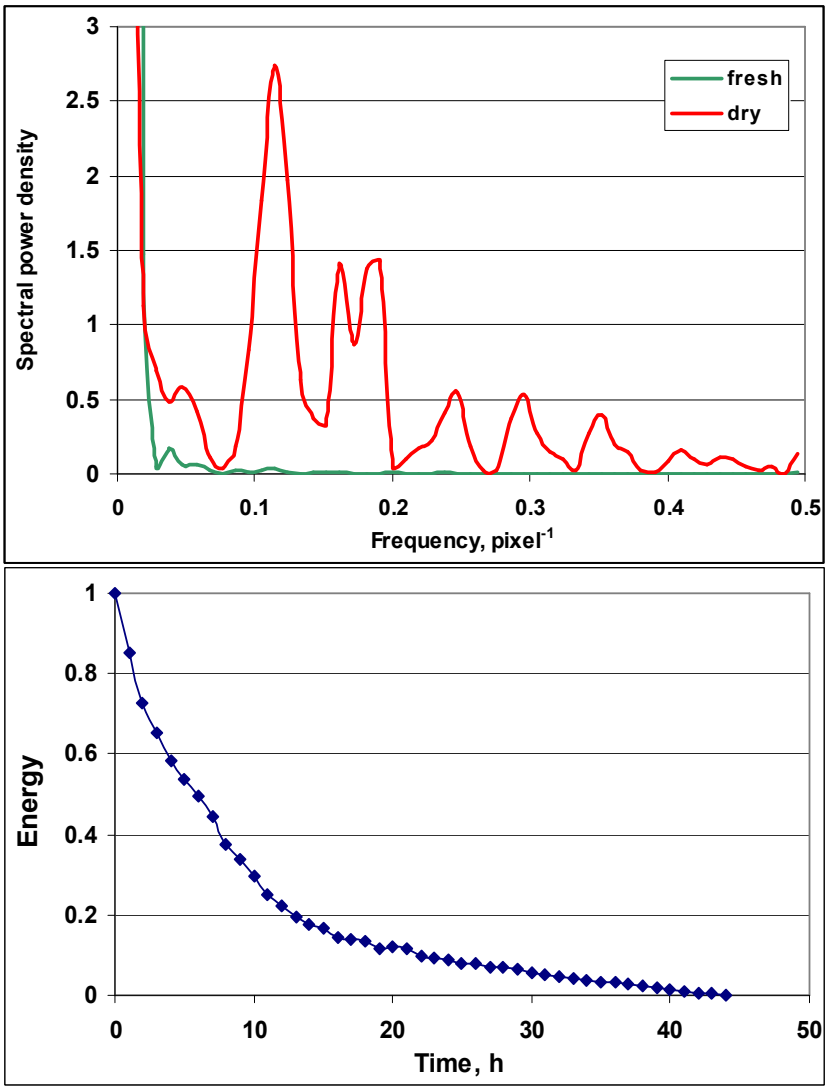

Figure 10. Spectral power density as a function of spatial frequency (FFT) for fresh (green) and dry (red) roots; b) Image energy vs time of drying

From Figure 10a it follows that fresh root does not have any high-frequency components, they appears in the process of shrinkage. For dried root there was a large spectral component, corresponding to frequency 0.1 $pixel^{-1}$. It can be related to wrinkles on the surface with the typical distance 10 pixels (0.1mm) between them.

It follows that textural feature analysis gives two pieces of information: about spectral power density with respect to spatial coordinate and about energy decay with time of drying. In general, decreasing of energy with time of ginseng drying is in good correspondence with results reported for apple disks drying *(Fernandez et al., 2005)*.

4. Evaluation of SAIF performance for feedback control

Intelligent computer-vision system for automated inspection of food safety and quality (SAIF) was developed as re-configurable machine-vision software for monitoring, identification and control applications on the basis of NI-IMAQ Vision Builder 6.1. SAIF was tested as a part of knowledge-based control system. It offers an extensive set of optimized functions for advanced image processing, machine vision, pattern matching, blob analysis, spatial measurements and calibration of food products. Also it includes the ability to set up complex pass/fail decisions in order to control digital I/O devices such as PLC.

Performance of SAIF was tested in industrial conditions on ginseng batch dryer. Output of computer-vision system delivered information about area, colour and texture of ginseng in the batch. Subsequent image processing was done with IMAQ Histogram VI, using a procedure of centre-of-gravity averaging. Information about area changes in the process of drying was used for calculation of shrinkage kinetics and next conversion into moisture kinetics with model (equation 5). Both moisture estimate $m(t)$ and error $e_m(t)$ were used as dynamic variables in global control loop. Global control loop with computer-vision input provided observability of technological process of ginseng drying due to advanced

image processing and analysis. Colour degradation was estimated as an independent dynamic variable with another model (see Figure 7). This estimate was used in global control loop to prevent quality degradation below specified threshold. Ginseng quality was estimated on the basis of all available information. Errors for estimation of moisture content $\boldsymbol{e_m}$, quality e_q and drying rate $\boldsymbol{e_k}$ were calculated as discrepancy between estimation from observer and direct measurements.

Additionally, the user-friendly graphical interface with operator was developed. Operator was able to specify drying conditions (temperatures for each stage of drying, relative humidity, air velocity, size), initial, equilibrium and critical moisture contents, as well as the rate of image sampling. Online estimates of shrinkage, colour and moisture content on each stage of drying were displayed online on the screen. The quality of ginseng in drying process was indicated as “EXCELLENT”, “HIGH”, “SATISFACTORY” or “NON_SATISFACTORY”. If error in quality assessment was within allowable threshold, then “DRYING IN PROGRESS” was displayed. Otherwise it was displayed “CORRECTION” and correction of drying regime was required.

5. Conclusions

Experimental testing of computer vision system (SAIF) for ginseng drying showed advantages of SAIF for online monitoring of important state variables, such as moisture, colour and texture. Moisture was identified from morphological attributes (area), using relationship between area shrinkage and volumetric moisture content with 8% error and 95% confidence. Color was identified as color intensity in HSI colour space. Wrinkles were identified from spectral analysis as the result of FFT with following filtering of spectral harmonics. SAIF was also used for automated inspection of final product quality.

Our research results demonstrated the feasibility of SAIF as an accurate online observer for a closed-loop food processing. Data extracted from image analysis represent both quality factors perceived by consumers (color, texture) and process parameters (moisture content, drying rate), important for control purposes.

References

1. Batchelor, B.C., Hill, D.A., Hodgson, D.C. 1985. *Automated visual inspection.* London, UK: IFS (Publications), Ltd.
2. Blasco, J., Aleixos, N., Molto E. 2003. Machine-vision system for automatic quality grading of fruit. *Biosystems Engineering 85* (4), 415-423.
3. Davidson V.J., Li X., Brown R.B. (2004). Forced-air drying of ginseng roots: 1. Effects of air temperature on quality. J. Food Engineering, 63: 361-367.
4. Fernandez, L., Castillero, C., Aguilera, J.M. 2005. An application of image analysis to dehydratation of apple discs. *Journal of Food Engineering,* **67**, 185-193.
5. Graves M., Batchelor B.G., Lee M. L. 2003. Machine Vision for the Inspection of Natural Products. Springer Verlag. 491p.
6. Gunasekaran S. 2000. Nondestructive Food Evaluation: Techniques to Analyze Properties and Quality. Marcel Dekker, 2000. 423p**.**
7. Gunasekaran, S., 1996. Computer vision technology for food quality assurance. *Trends in Food Science & Technology,* 7 (8), 245-256.
8. Jayas, D.S., Paliwal J., Visen N.S. 2000. Multi-layer neural networks for image analysis of agricultural products. *Journal of Agricultural Engineering Research,* **77** (2), 119-128.
9. Klir, G.J. 1985. Architecture of systems problem solving. Plenum Press. New York, London.
10. Ling P.P., Ruzhitsky V.N., Kapanidis A.N., Lee T.C. 1996. Chemical markers for the quality of processed and storage foods. *American Chemical Symposium Series, 631: 253-278. American Chemical Society, Washington DC.*
11. Liu, J.; Paulsen, M. R., 1997. Corn whiteness measurement and classification using machine vision. In: *1997 ASAE Annual International Meeting Technical Papers*, Paper No. 973045, ASAE, 2950 Niles Road, St. Joseph, Michigan 49085-9659, USA.
12. Lotch, P., 1997. Full colour image analysis as a tool for quality control and process development in the food industry. In: *1997 ASAE Annual International Meeting Technical Papers*, paper No. 973006, ASAE, 2950 Niles Road, St. Joseph, Michigan 49085-9659, USA.

13. Lu W., Sun D.W. 2000. Computer vision systems for rapid quality inspection of agricultural and food products. *In: Technology Innovation and Sustainable Agriculture ICETS 2000, p.201-206.*

14. Majumdar, S; Jayas, D. S. (2000a). Classification of cereal grains using machine vision. I. Morphology models. *Transactions of ASAE, **43**(6),* 1669-1675.
15. Majumdar, S; Jayas, D. S. (2000b). Classification of cereal grains using machine vision. II. Color models. *Transactions of ASAE, **43**(6),* 1677-1680.
16. Majumdar, S; Jayas, D. S. (2000c). Classification of cereal grains using machine vision. III. Texture models. *Transactions of ASAE, **43**(6),* 1681-1687.
17. Majumdar, S; Jayas, D. S. (2000d). Classification of cereal grains using machine vision. IV. Combined morphology, color and texture models. *Transactions of ASAE, **43**(6),* 1689-1694.
18. Ni, B.; Paulsen, M. R.; Reid, J. F., 1997. Size grading of corn kernels with machine vision. In: *1997 ASAE Annual International Meeting Technical Papers*, Paper No. 973046, ASAE, 2950 Niles Road, St. Joseph, Michigan 49085-9659, USA.
19. Paliwal, J., Visen, N.S., Jayas, D.S., White, N.D.G. 2003. Comparison of a neural network and a non-parametric classifier for grain kernel identification. *Biosystems Engineering **85**(3). 405-413.*
20. Rigney, M. P.; Brusewitz, G. H.; Kranzler, G. A., 1992. Asparagus defect inspection with machine vision. In: *Food Processing Automation II Proceedings of the 1992 Conference*. ASAE, 2950 Niles Road, St. Joseph, Michigan 49085-9659, USA.
21. Ruan, R.; Ning, S.; Ning, A.; Jones, R.; Chen, P. L., 1997. Estimation of scabby wheat incident rate using machine vision and neural network. In: *1997 ASAE Annual International Meeting Technical Papers*, Paper No. 973042, ASAE, 2950 Niles Road, St. Joseph, Michigan 49085-9659, USA.
22. Sonka, M; Hlavac, V; Boyle, R., 1999. Image Processing, Analysis, and Machine Vision. PWS publishing, California, USA.
23. Sun, D. W., 2000. Inspecting pizza topping percentage and distribution by a computer vision method. *Journal of Food Engineering,* **44**, 245-249.
24. Tao, Y.; Heineman, P. H.; Varghese, Z.; Morrow, C. T.; Sommer III, H. J., 1995. Machine vision for colour inspection of potatoes and apples. *Transaction of the ASAE,* **38** (5), 1555-1561.
25. Zuech, N., 1990. Applying machine vision in the food industry. In: *Food Processing Automation Proceeding of the 1990 Conference,* ASAE, 2950 Niles Road, St. Joseph, Michigan 49085-9659, USA.